

Minimization and Optimum Distribution of Entropy Generation for Maximum Net Power Output of the Small-Scale Open and Direct Solar Thermal Brayton Cycle

W.G. Le Roux, T. Bello-Ochende and J.P. Meyer
Department of Mechanical and Aeronautical Engineering, University of Pretoria

Abstract

A heat source can be considered as the Brayton cycle's life support. This heat source need not be from combustion, which is mostly the case, but can be extracted from solar energy. The irreversibilities of the solar thermal Brayton cycle are mainly due to heat transfer across a finite temperature difference and fluid friction. The optimum geometry of the receiver and recuperator can be established by maximizing the net power output of the system. In this paper the Second Law of Thermodynamics and entropy generation minimization is applied to optimize the component geometries. The dynamic trajectory optimization method is used. Standard micro-turbines and a range of concentrator radii are considered. Results show the optimum operating conditions and minimum entropy generation as a function of system mass flow rate. For a system with an optimized geometry and an optimized operating condition, the solar receiver is the main contributor to the total rate of entropy generation and the irreversibilities are spread throughout the system in such a way that the internal irreversibilities are almost three times more than the external irreversibilities. For a specific environment and parameters there exists an optimum receiver and recuperator geometry such that the system produces maximum net power output.

Keywords: solar, Brayton, optimization, recuperator, receiver

1. Introduction

South Africa, like Southern Africa, has a lot of potential to generate large amounts of its power from solar technologies. Concentrated solar power systems utilize the concentrated power of the sun as a heat source to drive a power-generating turbine. The Brayton cycle generates power with the use of a gas working fluid. For a water-scarce country like South Africa, the Brayton cycle seems very attractive. Fluri (2009) showed that the total potential generation capacity of CSP (Concentrated Solar Power) in South Africa, is more than 500 GW. Mills (2004) envisaged that emphasis may shortly shift to solarised Brayton micro-turbines from Dish-Stirling technology due to high Stirling engine costs. Chen et al. (2007) compared the efficiency of the Brayton cycle with those of other power cycles and found that it is definitely worth studying. The highest-efficiency Brayton cycles are regenerative cycles with low pressure ratios. Counterflow heat exchangers should be used as recuperators (Shah, 2005) and is recommended for solar-thermal application (Kreith and Kreider, 1978). According to Bejan (1982) counterflow heat exchangers finds numerous applications in regenerative heating associated with Brayton cycles. Shah (2005) regards the Honeywell turbo-machinery as worth mentioning when it comes to their development expertise in micro-turbines in recent history.

The Brayton cycle usually requires large receivers or cavity receivers due to low gas heat transfer coefficients. A black solar receiver, mounted at the focus of a parabolic dish concentrator can be sized such that it absorbs the maximum amount of heat (Stine and Harrigan, 1985). Convection losses can be drastically reduced by employing a receiver mounted in a cavity and selective coating for reducing the thermal losses due to radiation. Different classical cavity geometries were investigated by Shuai et al. (2008). Prakash et al. (2009) investigated heat losses from a solar cavity receiver at different inclination angles of head-on and side-on winds and found that the thermal and optical losses occurring from an open cavity solar receiver are less when compared to other

types of receivers. Reddy and Sendhil Kumar (2008) compared different types of cavity receivers numerically and found that their modified cavity receiver experiences lower convection heat losses than the other receivers and suggest that it may be preferred in a solar dish collector system. A numerical investigation of natural convection heat loss (Sendhil Kumar and Reddy, 2007), an inclusion of the contribution of radiation losses (Reddy and Sendhil Kumar, 2008) and an improved model for natural convection heat loss was presented for the modified cavity (Reddy and Sendhil Kumar, 2009).

Bejan (1982), Bejan et al. (1996) and Oğulata et al. (2000) state that the irreversibilities of convective heat transfer are due to heat transfer across a nonzero temperature difference and fluid friction. For a heat exchanger, Yilmaz et al. (2001) include the losses due to the heat exchange with the environment. Bejan (1982) proposed ways of reducing irreversibility production in heat exchangers. For a solar receiver configuration, Bejan (1982) mentioned three main features that cause thermodynamic irreversibilities in its operation: sun-receiver heat-exchange, receiver-ambient heat loss and the internal irreversibility in the receiver. According to the Gouy-Stodola theorem the maximization of exergy output is identical to the minimization of total entropy generation "*in the column of cross-section extending from the environment temperature (T_0) to the apparent sun temperature as an exergy source (T^*)*" (Bejan, 1982, p. 213). Bejan (1997) investigated the entropy generation rate involved with the transformation of monochromatic radiation into blackbody radiation and scattering.

An optimal receiver temperature for maximum power per unit area can be determined in three ways: by maximizing the net power output, minimizing the entropy generation rate, or by maximizing the exergy streaming (Bejan, 1997). The total rate of entropy generation can be minimized by selecting the physical dimensions of heat exchanger surfaces to get the best optimal design that fits a particular application. Entropy generation minimization (EGM) has been used in various internal flow optimization studies such as: The optimum tube diameter or Reynolds number for a tube (Bejan, 1982 and Bejan et al., 1996); The optimal Reynolds number for single-phase, fully developed, laminar and turbulent flow with constant heat flux (Ratts and Raut, 2004); and the optimum channel geometries with constant wall temperature or constant heat flux (Zimparov et al., 2006a, 2006b and 2006c). Entropy generation and its minimization has also been expressed for numerous heat exchangers and heat transfer surfaces: counterflow and nearly-ideal heat exchanger neglecting fluid friction (Sarangi and Chowdhury, 1982), tubular heat exchangers (Cornelissen and Hirs, 1997 and Zimparov, 2001), heat exchangers restricted to perfect gas flows (Hesselgreaves, 2000), balanced cross-flow recuperative plate type heat exchanger with unmixed fluids (Oğulata et al, 2000); and a parallel-plates ideal gas counterflow heat exchanger (Ordóñez and Bejan, 2000). Hesselgreaves (2000), Oğulata et al. (2000) and Ordóñez and Bejan (2000) suggest the use of the ϵ - NTU method, based on the Second Law of Thermodynamics, to get the outlet temperatures and the total heat transfer from the hot fluid to the cold fluid. Heat exchanger optimization using EGM has been utilized in various applications: A thermoacoustic engine (Ishikawa and Hobson, 1996); A condenser in a vapor-compression-cycle refrigeration system for environmental control of aircraft (Shiba and Bejan, 2001); and cryogenics (Lerou et al., 2005).

Exergetic analysis in solar thermal application has been done by Narendra et al. (2000) and Jubeh (2005). These analyses were respectively done for a solar thermal Rankine heat engine and a regenerative Brayton cycle with isothermal heat addition and isentropic compressor and turbine. Various authors have emphasised the importance of the optimization of the global performance of a system, by minimizing the sum of the irreversibilities from all the different components or processes of the system (spreading the entropy generation rate through the system by optimally sizing the hardware, in stead of optimizing components individually). These authors include Zimparov et al.

(2006, p. 1620 and p. 4840), Bejan (1996 and 1997), Bejan et al. (1996, p. 5), Shiba and Bejan (2001) and Ordóñez and Bejan (2000).

The purpose of this paper is to optimally size the geometry of a cavity receiver and recuperator in a recuperative solar thermal Brayton cycle, such that the system produces maximum net power output. Systems producing a net power output of 2-100 kW are analyzed. An analysis will be done by looking at the solar thermal power system as a whole and minimizing the entropy generation rate through the whole system, instead of optimizing components individually. This holistic view can hold valuable data and understanding into the optimal distribution of entropy generation throughout the small-scale recuperative Brayton cycle. The dynamic trajectory optimization method is used to get the optimum receiver and recuperator geometries. Standard micro-turbines are used in the analysis, which keeps the study relevant and useful.

2. Model

The open and direct solar thermal Brayton cycle using a recuperator is shown in Fig. 1.

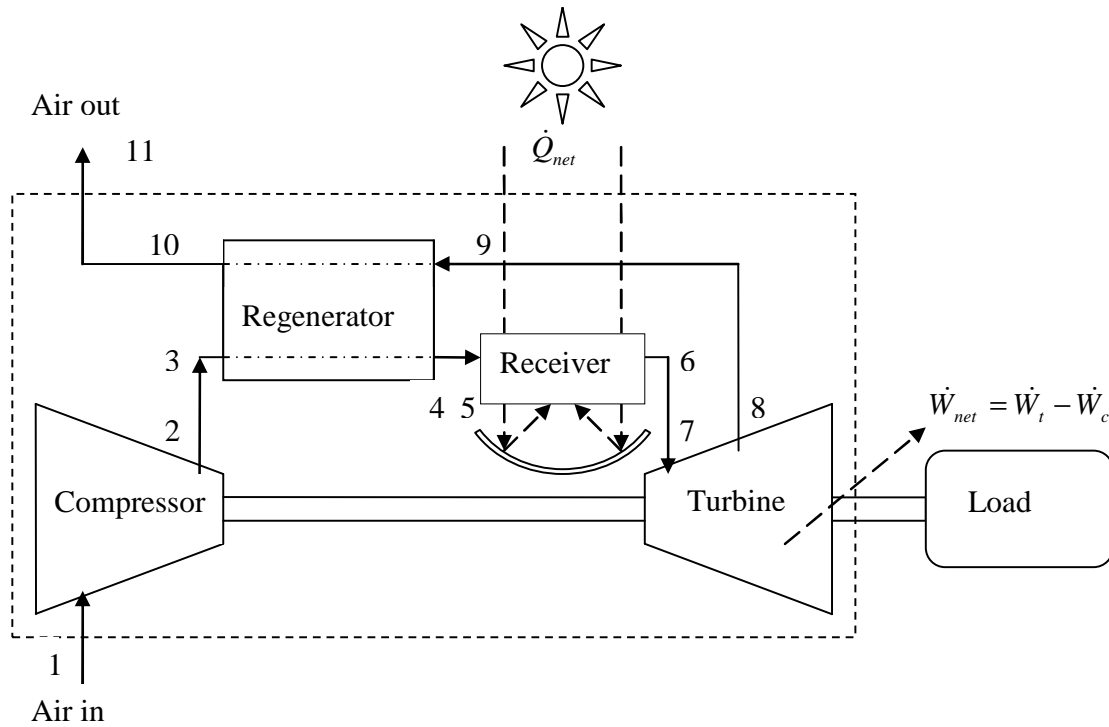


Figure 1. The open and direct solar thermal Brayton cycle using recuperation

2.1. Solar collector and receiver

The collector consists of a parabolic concentrator and modified cavity receiver proposed by Reddy and Sendhil Kumar (2009). The convection heat loss takes place through the receiver aperture. An area ratio of 8 (receiver inner wall area, A_w , to aperture area, A_a) is recommended by Reddy and Sendhil Kumar (2009) as it was found to be the ratio that gives the minimum heat loss. Since the surface area of a sphere is $4\pi r^2$, it is assumed that the radius of the receiver can be calculated with Eq. 1.

$$r = \sqrt{(A_w + A_a)/3\pi} = D/2 \quad (1)$$

The receiver inner surface is made up of closely wound copper tubing with diameter, $D_{h,rec}$, and length, L_{rec} . These tubes are placed very closely to touch each other to form a continuous hemispherical surface. The working fluid is pumped concentrically through these tubes, as can be seen in Fig. 2. For minimum heat loss Eq. 2 arises.

$$r = \sqrt{3}W_n / 2 \quad (2)$$

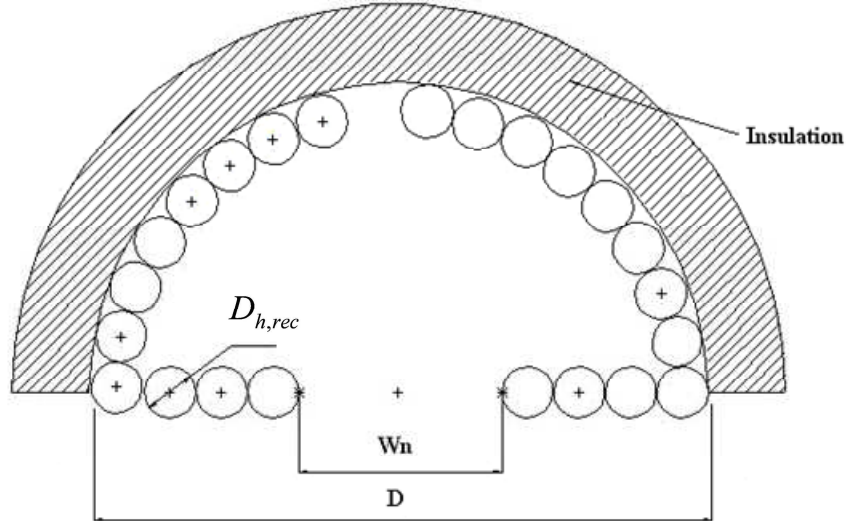


Figure 2. Geometry of the cavity receiver used in the analysis

The aperture diameter (W_n) is calculated with Eq. 3 since $A_w = D_{h,rec}L_{rec}$.

$$W_n = \sqrt{D_{h,rec}L_{rec} / 2\pi} \quad (3)$$

According to Reddy and Sendhil Kumar (2008) the ratio of radiation heat loss to convection heat loss is a function of receiver inclination and varies between approximately 0.9 and 1.33. For this analysis it is assumed that $\dot{Q}_{loss-rad} \approx \dot{Q}_{loss-conv}$ or $\dot{Q}_{loss} \approx 2\dot{Q}_{loss-conv}$ for the modified cavity receiver. From Reddy and Sendhil Kumar (2009, p. 1889), and for $A_w / A_a = 8$, the Nusselt number for a 3-D receiver model can be calculated using Eq. 4, where β is the receiver inclination, k is the thermal conductivity of air and Gr_D is the Grashof number based on the receiver diameter (D).

$$Nu_D = h_{conv}D / k = 0.698Gr_D^{0.209}(1 + \cos \beta)^{0.968}(T_w / T_\infty)^{-0.317}(W_n / D)^{0.425} \quad (4)$$

Eq. 5 shows the total heat loss from the wall temperature (T_w) to the surroundings (T_∞).

$$\dot{Q}_{loss} = 2h_{conv}A_a(T_w - T_\infty) \quad (5)$$

2.1.1. Sizing of receiver aperture

The sizing algorithm of Stine and Harrigan (1985) is used for receiver aperture sizing. The sizing algorithm uses the collector area, rim angle (ψ_{rim}), specular reflectance, inclination, irradiance, parabolic concentrator error and heat loss to determine the net absorbed heat as a function of the receiver aperture diameter. Starting at a rim angle of

0° through to an angle of ψ_{rim} , in increments of 1°, the amount of intercepted solar energy per segment of collector area is computed for a range of aperture diameters using a flux capture fraction with standard deviations of the total angular error. The total absorbed heat is the total intercepted energy minus the total heat loss. The amount of heat absorbed, \dot{Q}_{net} , is a function of the cavity aperture diameter, W_n . This function can be numerically approximated with the Discrete Least Squares Approximation Method (Burden and Faires, 2005, p. 482) and is shown in Eq. 6.

$$\dot{Q}_{net} = \sum_{i=0}^{10} a_i W_n^i \quad (6)$$

There exists an aperture diameter which absorbs a maximum amount of solar energy for the system. The specific aperture size is coupled to the receiver's channel dimensions (its length, and tube diameter). The shadow of the receiver and its insulation (as a function of aperture size) is also accounted for when calculating the available energy at the receiver. Heat loss through conduction at the cavity receiver through the insulation is usually small. It was assumed that the conduction heat loss is 10% of the sum of the radiation and convection heat loss.

2.2. Recuperator

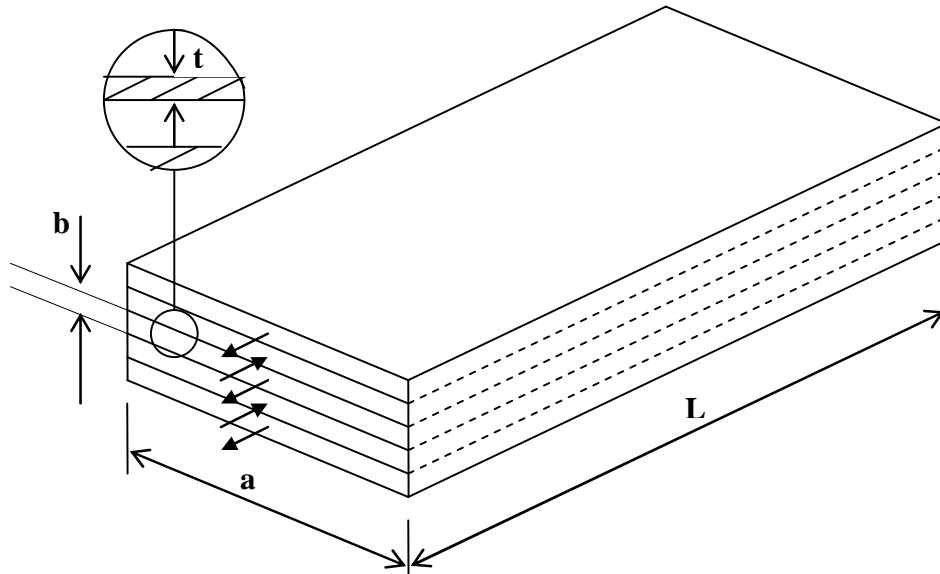


Figure 3. Geometry of recuperator channels

A counter-flow plated recuperator is used. The design and assembly will be as simply illustrated in Fig. 3, where only a few plates are stacked to create flow channels. The geometry variables for the recuperator to be optimized are the channel hydraulic diameter, D_h , tube length, L , and aspect ratio, a/b . A single channel has a divided mass flow rate and $A_s = 2aL$. The regenerator efficiency can be calculated using the ϵ -NTU method. The number of channels (n) in the recuperator depends on the recuperator height (H), channel height (b) and thickness of the channel separating surface (t). For the analysis $t = 1$ mm. Thus the number of channels can be determined with Eq. 7.

$$n = H / (t + b) = H / (t + D_h (a/b + 1) / (2(a/b))) \quad (7)$$

Eq. 8 gives the mass flow rate per channel.

$$\dot{m} = 2\dot{m}_{system} / n \quad (8)$$

The surface area (A_s) for a channel is given in Eq. 9.

$$A_s = 2(a+b)L = D_h L \left(\left(\frac{a}{b} \right) + 1 \right) \left(1 + \left(\frac{a}{b} \right)^{-1} \right) \quad (9)$$

For the recuperator the Reynolds number for a rectangular channel is shown in Eq. 10.

$$Re = (4(a/b)\dot{m}) / (\mu D_h (a/b + 1)^2) \quad (10)$$

The Gnielinski equation (Eq. 11) (Gnielinski (1976), cited in Çengel (2006)) can be used to determine the Nusselt number since small Reynolds numbers are most likely to be present. The Petukhov equation (Eq. 12) (Petukhov (1970), cited in Çengel (2006)) is used to calculate the friction factor. Pr is the Prandtl number.

$$Nu_D = (\text{Pr}(Re-1000)(f/8)) / \left(1 + 12.7(f/8)^{0.5} \left(\text{Pr}^{2/3} - 1 \right) \right) \quad (11)$$

$$f = (0.79 \ln Re - 1.64)^{-2} \quad (12)$$

The recuperator efficiency is calculated using the ε - NTU method with the fouling factor, $R_f = 0.004$. With the use of the friction factor, and the definition of the pressure drop, Eq. 13 arises, where μ is the dynamic viscosity and ρ is the density of the fluid.

$$\Delta P = \left(0.79 \ln \frac{4\dot{m}(a/b)}{\mu D_h (a/b + 1)^2} - 1.64 \right)^{-2} \left(\frac{8\dot{m}^2 (a/b)^2}{\rho (a/b + 1)^4} \right) (L / D_h^5) \quad (13)$$

2.3. Compressor and turbine

Standard micro-turbines are considered for the analysis. According to Snyman (2009), the pressure ratio ($r = P_2 / P_1$) should be chosen to be a parameter when considering geometric optimization. The mass flow rate through the system depends on the compressor, which in turn depends on the turbine. The compressor efficiency, mass flow rate and pressure ratio, are intrinsically coupled to each other - as can be seen from standard micro-turbines (Garrett, 2009). The compressor pressure ratio as a parameter fixes the mass flow rate and compressor efficiency as parameters. The highest compressor efficiency is on the island in the middle of a compressor map (between two mass flow rate values: \dot{m}_{low} and \dot{m}_{high} , and between two pressure ratio values: r_{low} and r_{high}). The pressure ratio (r) – mass flow rate (\dot{m}) relation can be approximated with a straight line on this island (Eq. 14).

$$\dot{m} = \left((\dot{m}_{high} - \dot{m}_{low}) / (r_{high} - r_{low}) \right) (r - r_{low}) + \dot{m}_{low} \quad (14)$$

An optimum pressure ratio, for a specific micro-turbine, exists which would (with its optimized geometry) give the maximum net power output for the system. An objective

function in terms of variable geometry (using geometry variables from all over the system) can now be compiled using parameters. The maximum of the objective function can then be found at different parameter values.

2.4. Temperature and pressure fields

Before constructing the objective function, the temperature and pressure fields must be known. The assembly of these fields requires an iteration. Firstly, $T_1 = 300$ K and $P_1 = 80$ kPa (see Fig. 1). The temperatures and pressures in all the ducts are calculated with an assumed temperature loss or pressure drop which is small. The iteration starts off with $T_5 = 800$ K. Eqs. 15, 16, 17 and 18 and the recuperator efficiency are employed to calculate the remaining unknowns.

$$T_6 = \left(\sum_{i=0}^{10} a_i \sqrt{D_{h,rec} L_{rec} / 2\pi}^i \right) / \dot{m} c_p + T_5 \quad (15)$$

$$P_4 = P_3 - \left(0.79 \ln \frac{4\dot{m}_{channel} (a/b)}{\mu D_h (a/b+1)^2} - 1.64 \right)^{-2} \left(\frac{8\dot{m}_{channel}^2 (a/b)^2}{\rho (a/b+1)^4} \right) \left(\frac{L}{D_h^5} \right) \quad (16)$$

$$P_6 = P_5 - \left(0.79 \ln \frac{4\dot{m}}{\mu \pi D_{h,rec}} - 1.64 \right)^{-2} \left(\frac{8\dot{m}^2}{\rho \pi^2} \right) \left(\frac{L_{rec}}{D_{h,rec}^5} \right) \quad (17)$$

$$P_9 = P_{10} + \left(0.79 \ln \frac{4\dot{m}_{channel} (a/b)}{\mu D_h (a/b+1)^2} - 1.64 \right)^{-2} \left(\frac{8\dot{m}_{channel}^2 (a/b)^2}{\rho (a/b+1)^4} \right) \left(\frac{L}{D_h^5} \right) \quad (18)$$

The iteration continues until the error is smaller than 0.001. When the iteration is done, the temperature and pressure fields are established and the objective function can be constructed.

2.5. The objective function

The Gouy-Stodola theorem states that the lost available work (exergy destruction) of a system is equal to the entropy generation in the control volume. Thus, when the maximum net power output that can be delivered by the system is required, the sum of the generated entropy rate in the system should be considered. The finite heat transfers and pressure drops in the compressor, turbine, recuperator, receiver and ducts are identified as entropy generation mechanisms. The entropy generation rate involved with the transformation of monochromatic radiation into blackbody radiation is neglected, since solar radiation falls in a wavelength band which is close enough to the minimum entropy generation as shown by Bejan (1997). For the analysis in this work, the equivalent temperature of the sun (T^*) as an exergy source, will be assumed to be 2470 K, so that the entropy generation due to scattering can be neglected. Scattering decreases the monochromatic radiation temperature of the sun to between 7 and 70% which causes entropy generation (Bejan, 1997).

When doing an exergy analysis for the system and assuming that the velocities and height at the inlet and outlet are equal ($V_1 = V_{11}$ and $Z_1 = Z_{11}$), the objective function can be assembled in terms of the temperature and pressure field. The function to be maximized (the objective function), is \dot{W}_{net} (the net power output). Eq. 19 shows the objective function in terms of the temperature and pressure fields. The entropy

generation rate for each component is added and is shown in block brackets. Note that each temperature and pressure shown below can be written in terms of the geometry variables as was explained in the previous section. Note that R is the gas constant and c_{p0} is the specific heat.

$$\begin{aligned}
\dot{W}_{net} = & \dot{Q}_{net} + \dot{m}c_{p0}(T_1 - T_{11}) - \dot{m}T_0c_{p0} \ln(T_1 / T_{11}) \\
& - T_0 \left[-\dot{m}c_{p0} \ln(T_1 / T_2) + \dot{m}R \ln(P_1 / P_2) \right]_{compressor} \\
& - T_0 \left[\dot{Q}_{loss} / T_0 + \dot{m}c_{p0} \ln(T_3 / T_2) - \dot{m}R \ln(P_3 / P_2) \right]_{Duct23} \\
& - T_0 \left[\dot{Q}_{loss} / T_0 + \dot{m}c_{p0} \ln(T_5 / T_4) - \dot{m}R \ln(P_5 / P_4) \right]_{Duct45} \\
& - T_0 \left[\dot{Q}_{loss} / T_0 + \dot{m}c_{p0} \ln(T_7 / T_6) - \dot{m}R \ln(P_7 / P_6) \right]_{Duct67} \\
& - T_0 \left[\dot{Q}_{loss} / T_0 + \dot{m}c_{p0} \ln(T_9 / T_8) - \dot{m}R \ln(P_9 / P_8) \right]_{Duct89} \\
& - T_0 \left[\dot{m}c_{p0} \ln \left[\frac{T_{10}T_4}{T_9T_3} \left(\frac{P_{10}P_4}{P_9P_3} \right)^{(1-k)/k} \right] + \dot{Q}_{loss} / T_0 \right]_{recuperator} \\
& - T_0 \left[\dot{m}c_{p0} \ln(T_6 / T_5) - \dot{m}R \ln(P_6 / P_5) \right]_{solarcollector} \\
& - T_0 \left[-\dot{m}c_{p0} \ln(T_7 / T_8) + \dot{m}R \ln(P_7 / P_8) \right]_{turbine} \tag{19}
\end{aligned}$$

2.6. Constraints

The concentration ratio between collector area and aperture area, $CR \geq 100$. Therefore

$$D_{h,rec} L_{rec} / 8 - A_s / 100 \leq 0 \tag{20}$$

Eq. 21 prevents that the receiver loses its cavity shape, by only allowing a minimum of two diameters in the distance between the aperture edge and the edge of the receiver.

$$2D_{h,rec} - \left((\sqrt{3} - 1) / 2 \right) \sqrt{D_{h,rec} L_{rec} / 2\pi} \leq 0 \tag{21}$$

The cavity receiver tubes are constructed using copper. The surface temperature of the receiver tubes should stay well below its melting temperature. A maximum temperature of 1200 K is identified for the analysis by considering Garrett (2009) and Shah (2005). The surface area of a channel and the Dittus-Boelter equation (Dittus and Boelter (1930), cited in Çengel (2006)) help to construct Eq. 22, which is the maximum surface temperature of the receiver.

$$T_s = T_6 + \dot{Q}_{net} / \left(0.023\pi L_{rec} k Pr^{0.4} \left(4\dot{m} / (\mu\pi D_{h,rec}) \right)^{0.8} \right) \tag{22}$$

The longer the recuperator the more beneficial it is to the system. There needs to be a constraint on its length. To make sure the system stays compact, the recuperator's length should not exceed the length of the radius of the dish.

3. Research Methodology

There are five geometric variables to be optimized: The cavity receiver tube diameter ($D_{h,rec}$), the tube length of the cavity receiver (L_{rec}), the hydraulic diameter of the recuperator channels (D_h), the length of the recuperator channels (L) and aspect ratio of the recuperator channels (a/b). The objective function (net power output of the system) in terms of the scaled geometry variables, parameters and constants is maximized using the dynamic trajectory optimization method by Snyman (2009) in MATLAB, with unit step size and convergence tolerance of 1×10^{-7} . The optimization algorithm, LFOPC by Snyman (2000, cited in Snyman, 2009, p. 101), requires the gradient of the objective function in each variable. The gradient of the function for each of the five variables in vector X , can be obtained with the derivative function where the step size, $h = 1 \times 10^{-8}$. Optimization of the geometry variables was done for each combination of the following parameters:

- a range of parabolic dish radii ($R = 3 - 9$ m)
- a range of micro-turbines from Garrett ($MT = 1 - 45$) each having its own range of pressure ratios (along the line of highest compressor efficiency on the compressor map of a specific micro-turbine).

A data point was created at each micro-turbine pressure ratio (in increments of 0.1) for each of the above combinations. Each data point represents an optimized system – a system with maximum net power output and optimized receiver and recuperator geometries. In Table 1 the default values can be seen, for which these results were generated.

Table 1. Values used for default analysis and for inspection

Environmental condition or parameter	Symbol	Default Value	Inspected value	Unit
Surrounding temperature	T_o	300	315	K
Average Irradiance (I)	I	1000	1200	W/m ²
Wind factor (w)	w	1 (no wind)	10	
Atmospheric Pressure	P_1	80 000	100 000	Pa
Concentrator rim angle	ϕ_{rim}	45	30	degrees
Receiver inclination	β	90	45	degrees
Recuperator Height	H	1	0.5	m

The effect on the optimum system, when each of these constants is changed individually, is also investigated and included in the results. Also note that the concentrator specular reflectivity is 0.93 and the concentrator error is 0.0067 mrad. The recuperator material has conductivity of 401 W/mK.

4. Results

Consider firstly the default settings. For all the optimized data points (all R , and all operating points of all the micro-turbines) the optimum recuperator channel mass flow rate behaves in a specific way relative to the mass flow rate of the system. This behavior can be seen in Fig. 4 (showing only $R = 4, 6$ and 8 m for clarity) and is explained in the following paragraph. Take note that each data point in Fig. 4 has an optimum geometry and gives maximum net power output at its specific mass flow rate. When inspecting Fig. 5 (again, $R = 3, 5, 7$ and 9 m are not shown, but behaved similarly), one can see that for all the data points, the optimum NTU increases as the system mass flow rate increases until it reaches its maximum. This means that it is most beneficial for a system with small mass flow rate, to have a small NTU. The following paragraph explains why.

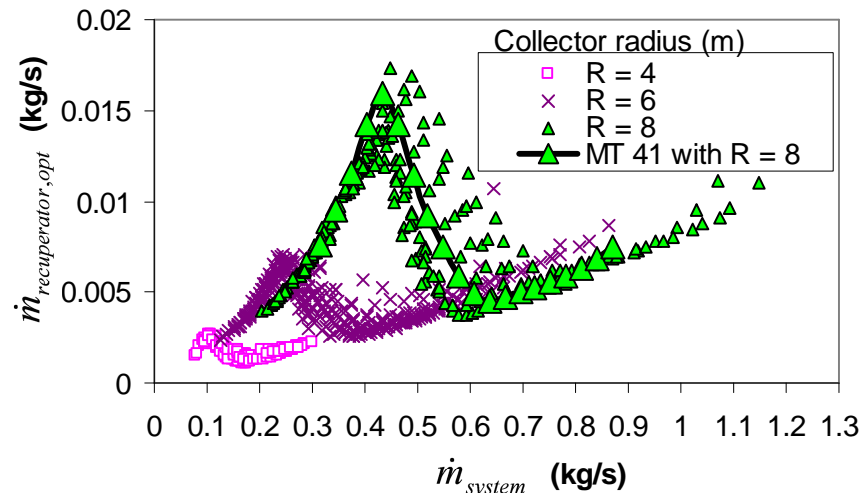


Figure 4. Optimum recuperator channel mass flow rate ($R = 4, 6 \text{ \& } 8 \text{ m}$)

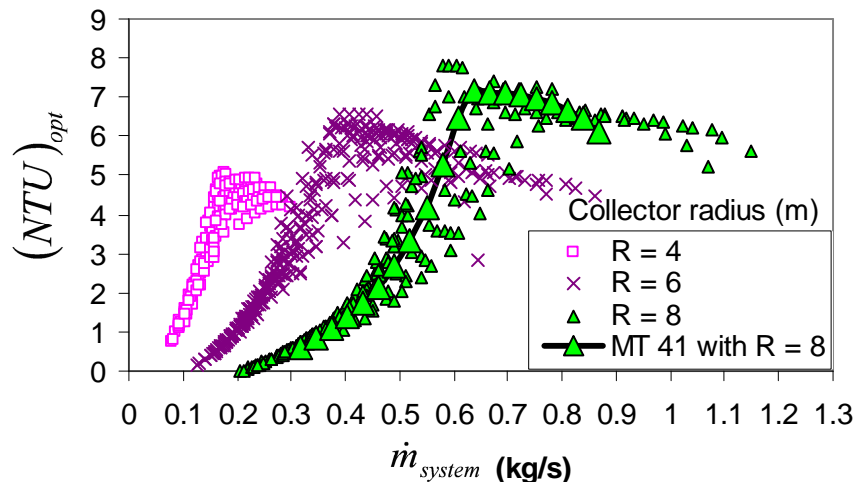


Figure 5. Optimum NTU for all data points ($R = 4, 6 \text{ \& } 8 \text{ m}$)

In Figs. 4 and 5, the specific data points for micro-turbine 41 with $R = 8 \text{ m}$ is shown. For this micro-turbine, the maximum net power output and minimum entropy generation rates are shown in Fig. 6. It shows how the irreversibilities are optimally spread out through the system. The behavior of this micro-turbine is explored, to better understand Figs. 4 and 5. The optimum external irreversibilities in Fig. 6 seem to be at a maximum when the mass flow rate is small. For high external irreversibilities, T_{11} must be high, which means that $\eta_{recuperator}$ should be small. This is why the optimum NTU is small at small mass flow rates as shown in Fig. 5. The optimum NTU increases as the mass flow rate increases. The optimized data shows that the small NTU is established with the use of a small surface area, large hydraulic diameter and large recuperator channel mass flow rate, which increases respectively until the maximum recuperator length constraint is reached (around 0.45 kg/s in Fig. 4). A large hydraulic diameter also keeps the pressure drop and fluid friction irreversibilities low for the recuperator. After the length constraint is reached, the recuperator mass flow rate and hydraulic diameter decreases as the mass flow rate increases, to ensure an increase in NTU. This is utilized until the friction irreversibilities grow too big at larger mass flow rates.

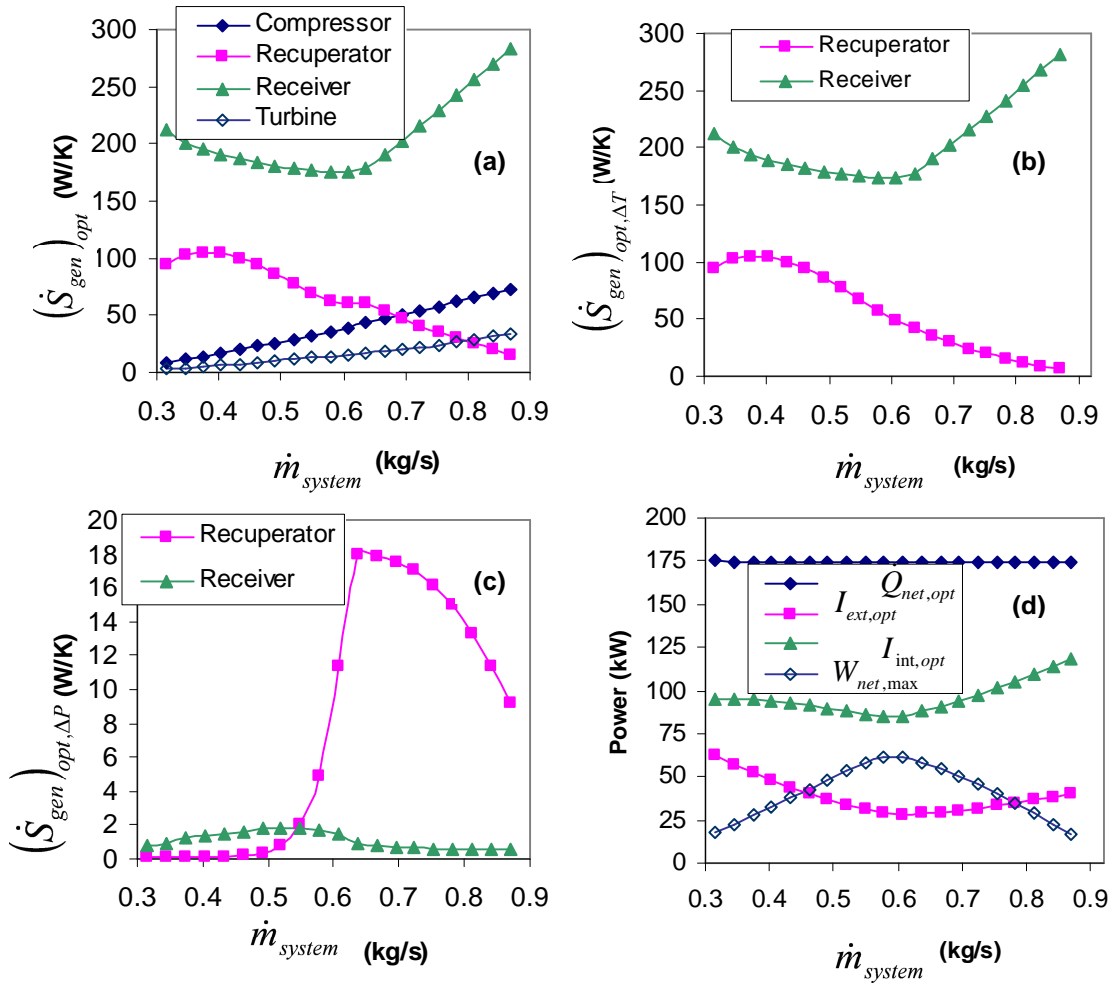


Figure 6. Optimized system (MT = 41, R = 8) : (a) – Total entropy generation rate. (b) – Contribution to total \dot{S}_{gen} due to temperature difference. (c) – Contribution to total \dot{S}_{gen} due to frictional pressure drop. (d) – Irreversibilities and available power

When considering the solar receiver irreversibilities (Fig. 6), it is clear that the receiver performs optimally when the irreversibilities due to friction are as small as possible. The downward irreversibility slope for the receiver is due to an increase in the NTU, which increases T_5 . The optimum T_6 goes to the maximum temperature it can be (due to maximum receiver surface temperature constraint), which means that the irreversibilities due to temperature difference in the receiver, can decrease as the mass flow rate increases. Eventually the NTU reaches its maximum (Fig. 5). For increasing mass flow rate, the irreversibilities due to temperature difference increases as a function of mass flow rate only. At the maximum NTU point, the recuperator channel mass flow rate is again utilized to be increased as the system mass flow rate increases, to keep the NTU at its maximum. In most of the cases, the maximum net power output in the operating range of the micro-turbine, was found at a mass flow rate close to this point or at higher mass flow rates. To keep the NTU constant, the hydraulic diameter is also kept constant, but increases slightly as the system mass flow rate increases, to keep the pressure drop irreversibilities small. This in turn forces the recuperator mass flow rate to also increase slightly as the system mass flow rate increases, as can be seen from Fig. 4. At the high mass flow rates it seems to be more beneficial for the system to have larger receiver

irreversibilities due to temperature difference. For this reason there is a decrease in the NTU (and T_5) at high mass flow rate.

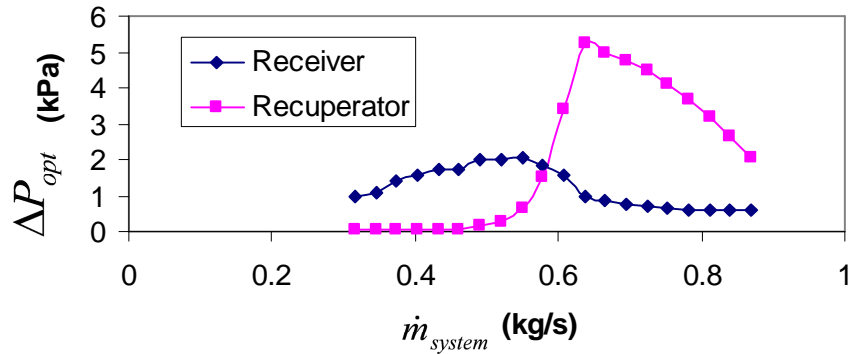


Figure 7. Optimum pressure drop in receiver and recuperator channel

Fig. 7 shows again the different phases of the system as a mass flow rate function of micro-turbine 41. It is interesting to note that for the optimum system, the pressure drop of the receiver is larger than the pressure drop in the recuperator when the mass flow rate is small. This changes at a specific mass flow rate, where after it is optimal for the recuperator pressure drop to be larger than the receiver pressure drop. Similar behavior was found for the other micro-turbines with $R = 8$ m.

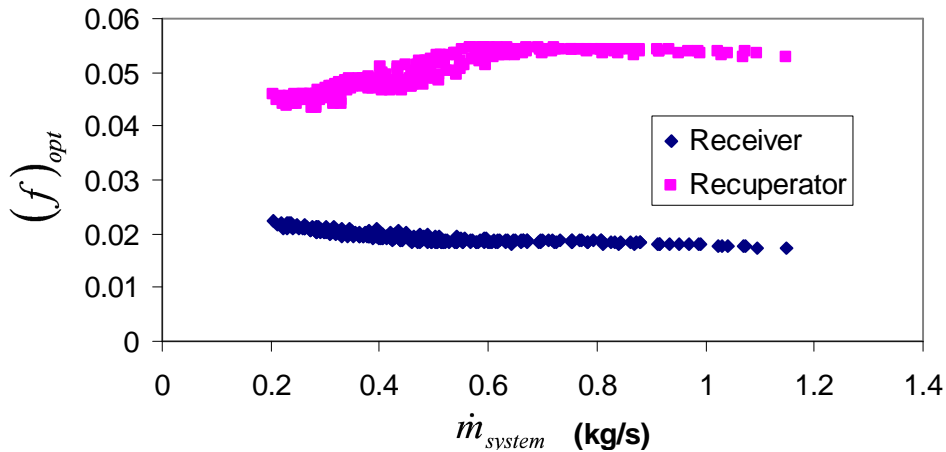


Figure 8. Optimum friction factor in receiver and recuperator

It was found that for $R = 8$ m, there exists an optimal friction factor for the receiver and recuperator flow channels, which was similar for each system using a different micro-turbine (Fig. 8). The optimum receiver friction factor decreases as a function of system mass flow rate while the recuperator friction factor increases, until it reaches a maximum where after it slowly decreases with system mass flow rate. The optimum recuperator friction factor is roughly 2.5 times larger than the optimum receiver friction factor.

From Fig. 6 it follows that the largest maximum net power output for the system (or optimum operating point) is at a point where the internal irreversibilities are approximately three times larger than the external irreversibilities. This result was also found for all the other combinations of collector radii and micro-turbines where a highest net power output could be identified. This result can be approximated for all collectors and micro-turbines with an optimum operating condition in this analysis with Eq. 23, where $C_W = (I_{int})_{opt} / (I_{ext})_{opt} \approx 3$.

$$-T_0 [\dot{S}_{gen}]_{int} \approx C_W [\dot{m} c_{p0} (T_{in} - T_{out}) - \dot{m} T_0 c_{p0} \ln(T_{in} / T_{out})]_{ext} \quad (23)$$

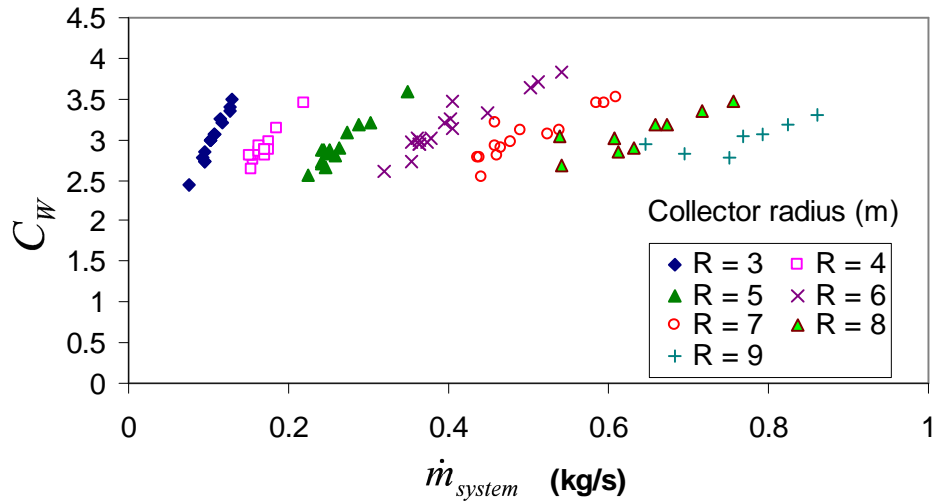


Figure 9. C_W as a function of the system mass flow rate

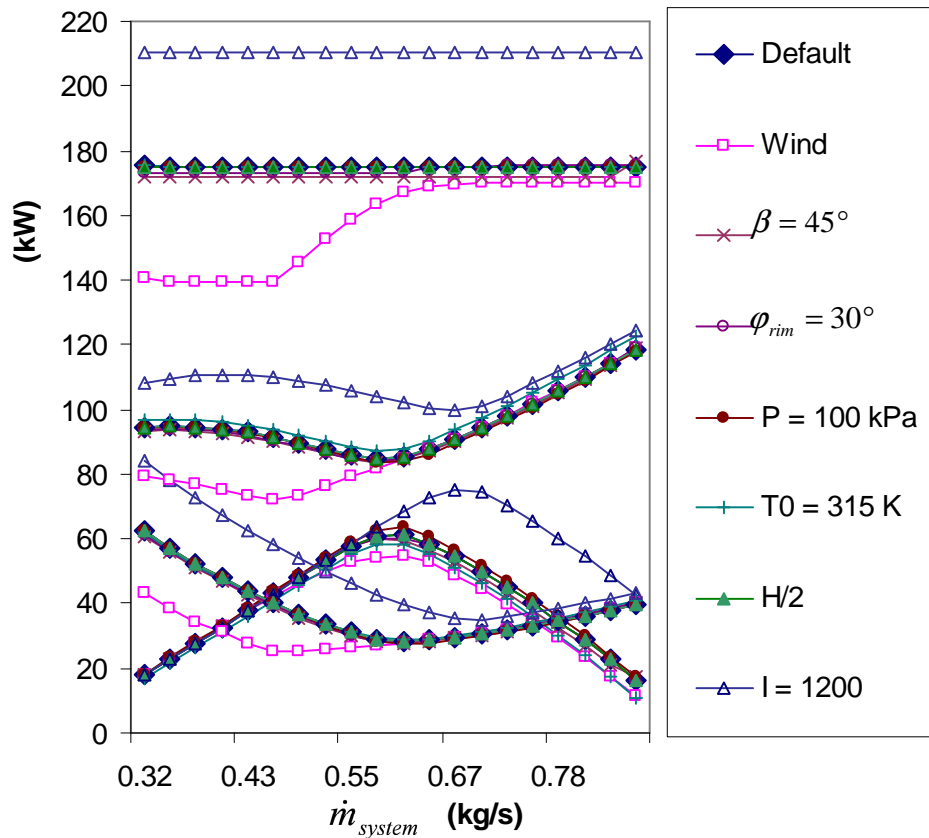


Figure 10. The effect of different conditions on the optimum performance of micro-turbine 41 and $R = 8$ m.

Fig. 9 shows that C_W mostly increases as the mass flow rate increases. The rate of increase decreases as the collector radius increases. Fig. 9 shows that $2.4 \leq C_W \leq 4$

depending on the mass flow rate. Other data points which are not at an optimum operating point, or close to one, do not fall in this range.

Fig. 10 shows the effect of environmental conditions and changed constants, on the optimum spreading of irreversibilities ($MT = 41$, $R = 8$ m). Note that from above and left in the figure the following are shown: Optimum absorbed heat, internal and external irreversibilities and maximum net power output. Most of these results did not differ much from the results of the default, however, usually the optimum geometry was changed to accommodate the change. Note that C_w is again approximately three, even for extreme conditions such as an irradiance of $1\ 200\ \text{W/m}^2$ and extreme wind. Also note how the wind effects the absorbed heat at smaller system mass flow rates. The wind calls for a smaller aperture diameter which constrains the amount of heat absorbed.

5. Conclusions and recommendations

Optimum recuperator and receiver geometries and optimum system operating conditions were established in the analysis, using the dynamic trajectory optimization method for different combinations of collector radius and standard micro-turbines. These results show how the irreversibilities are spread throughout the system optimally, so that the system can produce maximum power output. It was found that the optimum NTU increases with the system mass flow rate until it reaches a maximum, where after the NTU decreases slightly. A specific behavior of optimum recuperator channel mass flow rate as a function of system mass flow rate was seen as a result of optimum NTU behavior. It was noted that the internal irreversibilities of the optimized systems, were always more than the external irreversibilities. It was found that the maximum net power output is produced by the system when the internal irreversibilities are approximately three times more than the external irreversibilities. Results showed that the pressure drop of the receiver is larger than the pressure drop in the recuperator when the mass flow rate is small, but this changes around when the mass flow rate is large. An optimal friction factor for the receiver and recuperator flow channels was identified. The effect of environment and condition changes, on the optimal system performance, was investigated. Most of these results did not differ much from the results of the default, since the optimum geometry was changed to accommodate for external change. The results give insight into the optimal behavior and geometry of a small-scale, recuperative solar thermal Brayton cycle, limited to challenging constraints. These results can be considered in the preliminary stages of design.

References

- Bejan, A., 1982. *Entropy Generation through Heat and Fluid Flow*. Colorado: John Wiley & Sons, Inc.
- Bejan, A., Tsatsaronis, G. & Moran, M., 1996. *Thermal Design and Optimization*. New York: John Wiley & Sons, Inc.
- Bejan, A., 1997. *Advanced Engineering Thermodynamics*. 2nd ed. Durham: John Wiley & Sons, Inc.
- Burden, R.L. & Faires, J.D., 2005. *Numerical Analysis*. 8th ed. Youngston State University: Thomson Brooks/Cole.
- Çengel, Y.A., 2006. *Heat and Mass Transfer*. 3rd ed. Nevada, Reno: McGraw-Hill.
- Chen, L., Zhang, W. & Sun, F., 2007. Power, efficiency, entropy-generation rate and ecological optimization for a class of generalized irreversible universal heat-engine cycles. *Applied Energy*, 84, p.512-525.
- Cornelissen, R.L. & Hirs, G.G., 1997. Exergetic optimization of a heat exchanger. *Energy Conversion and Management*, 1, p.1567-1576.
- Dittus, F.W. & Boelter, L.M.K, 1930. *University of California Publications on Engineering* 2, p.433.

- Fluri, T.P., 2009. The potential of concentrating solar power in South Africa. *Energy Policy*, 37, p.5075–5080.
- Garrett, 2009. *Garrett by Honeywell: Turbochargers, Intercoolers, Upgrades, Wastegates, Blow-Off Valves, Turbo-Tutorials*. Available at: <http://www.TurboByGarrett.com> [accessed 26 April 2010]
- Gnielinski, V., 1976. New equations for heat and mass transfer in turbulent pipe and channel flow. *International Chemical Engineering*, 16, p.359-368.
- Hesselgreaves, J.E., 2000. Rationalisation of second law analysis of heat exchangers. *International Journal of Heat and Mass Transfer*, 43, p.4189-4204.
- Ishikawa, H. & Hobson, P.A., 1996. Optimisation of heat exchanger design in a thermoacoustic engine using a second law analysis. *International Communications in Heat and Mass Transfer*, 23, p.325-334.
- Jubeih, N.M., 2005. Exergy analysis and second law efficiency of a regenerative Brayton cycle with isothermal heat addition. *Entropy*, 7, p.172-187.
- Kreith, F. & Kreider, J.F., 1978. *Principles of Solar Engineering*. Colorado: Hemisphere Publishing Corporation.
- Lerou, P.P.P.M., Veenstra, T.T., Burger, J.F., ter Brake, H.J.M., Rogalla, H. 2005. Optimization of counterflow heat exchanger geometry through minimization of entropy generation. *Cryogenics*, 45, p.659-669.
- Mills, D., 2004. Advances in solar thermal electricity technology. *Solar Energy*, 76, p.19-31.
- Narendra, S., Kaushik, S.C., Misra, R.D., 2000. Exergetic analysis of a solar thermal power system. *Renewable Energy*, 19, p.135-143.
- Oğulata, R.T., Doba, F., Yilmaz, T., 2000. Irreversibility analysis of cross flow heat exchangers. *Energy Conversion & Management*, 41, p.1585-1599.
- Ordóñez, J.C., Bejan, A., 2000. Entropy generation minimization in parallel-plates counterflow heat exchangers. *International Journal of Energy Research*, 24, p.843-864.
- Petukhov, B.S., 1970. Heat transfer and friction in turbulent pipe flow with variable physical properties. *Advances in Heat Transfer*, 6.
- Prakash, M, Kedare, S.B. & Nayak, J.K., 2009. Investigations on heat losses from a solar cavity receiver. *Solar Energy*. 83, p.157-170.
- Ratts, B.E. & Raut, A.G., 2004. Entropy generation minimization of fully developed internal flow with constant heat flux. *Journal of Heat Transfer*, 126, p.656-659.
- Reddy, K.S. & Sendhil Kumar, N., 2008. Combined laminar natural convection and surface radiation heat transfer in a modified cavity receiver of solar parabolic dish. *International Journal of Thermal Sciences*. 47, p.1647–1657.
- Reddy, K.S. & Sendhil Kumar, N., 2009. An improved model for natural convection heat loss from modified cavity receiver of solar dish concentrator. *Solar Energy*. 83, p.1884–1892.
- Sarangji, S. & Chowdhury, K., 1982. On the generation of entropy in a counterflow heat exchanger. *Cryogenics*, 22 (2), p.63-65.
- Sendhil Kumar, N. & Reddy, K.S., 2007. Comparison of receivers for solar dish collector system. *Energy Conversion and Management*, 49, p.812-819.
- Sendhil Kumar, N. & Reddy, K.S., 2007. Numerical investigation of natural convection heat loss in modified cavity receiver for fuzzy focal solar dish concentrator. *Solar Energy*. 81, p.846–855
- Shah, R.K. (2005) Compact Heat Exchangers for Microturbines. In *Micro Gas Turbines* (pp. 2-1 – 2-18). Educational Notes RTO-EN-AVT-131, Paper 2. Neuilly-sur-Seine, France: RTO. Available from: <http://www.rto.nato.int/abstracts.asp>.

- Shiba, T. & Bejan, A., 2001. Thermodynamic optimization of geometric structure in the counterflow heat exchanger for an environmental control system. *Energy*, 26, p. 493-511.
- Shuai, Y., Xia, X. & Tan, H., 2008. Radiation performance of dish solar concentrator/cavity receiver systems. *Solar Energy*. 82, p.13-21.
- Snyman, J.A., 2009. Practical Mathematical Optimization. Pretoria: University of Pretoria.
- Stine, B.S. & Harrigan, R.W., 1985, *Solar Energy Fundamentals and Design*. New York: John Wiley & Sons, Inc.
- Yilmaz, M., Sara, O.N. & Karsli, S., 2001. Performance evaluation criteria for heat exchangers based on second law analysis. *Exergy, an International Journal*, 1 (4), p.278-294.
- Zimparov, V., 2001. Extended performance evaluation criteria for enhanced heat transfer surfaces: heat transfer through ducts with constant heat flux. *International Journal of Heat and Mass Transfer*, 44, p.169-180.
- Zimparov, V.D., Da Silva, A.K. & Bejan, A., 2006. Thermodynamic optimization of tree-shaped flow geometries with constant channel wall temperature. *International Journal of Heat and Mass Transfer*, 49, p.4839-4849.
- Zimparov, V.D., Da Silva, A.K. & Bejan, A., 2006. Constructal tree-shaped parallel flow heat exchangers. *International Journal of Heat and Mass Transfer*, 49, p.4558-4566.
- Zimparov, V.D., Da Silva, A.K. & Bejan, A., 2006. Thermodynamic optimization of tree-shaped flow geometries. *International Journal of Heat and Mass Transfer*, 49, p.1619-1630.